JOURNAL OF GEOPHYSICAL RESEARCH, VOL. 113, D19108, doi:10.1029/2008JD010074, 2008

Click Here for Full Article

Historical isotope simulation using Reanalysis atmospheric data

K. Yoshimura,[1,2] M. Kanamitsu,[1] D. Noone,[3] and T. Oki[2]

Received 5 March 2008; revised 13 June 2008; accepted 20 July 2008; published 8 October 2008.

[1] In this paper we present a multidecadal and global three-dimensional stable water isotope data set. This is accomplished by incorporating processes of the stable water isotopes into an atmospheric general circulation model and by applying a spectral nudging technique toward Reanalysis dynamical fields. Unlike the global model simulations forced only by sea surface temperature (SST), the dynamical fields used in the simulation are never far from observation because the spectral nudging technique constrains large-scale atmospheric circulation to that of observation, and therefore the simulated isotopic fields are reasonably accurate over the entire globe for daily to interannual time scales. As a case in point, it is revealed that the current approach reproduces the Arctic Oscillation much more correctly than the simulations forced only by SST, and consequently, the monthly isotopic variability better matches observations over midlatitudes to high latitudes in the Northern Hemisphere, especially Europe. This method is of great use in providing information in regions where in situ isotope observations are not available. Such information is required for a variety of biogeochemical, hydrological, and paleoclimate studies and as boundary and initial conditions for regional isotopic simulations.

Citation: Yoshimura, K., M. Kanamitsu, D. Noone, and T. Oki (2008), Historical isotope simulation using Reanalysis atmospheric data, *J. Geophys. Res.*, *113*, D19108, doi:10.1029/2008JD010074.

1. Introduction

[2] Stable oxygen and hydrogen isotopes in water ($H_2^{18}O$ and HDO) are useful natural tracers for hydrologic cycles [e.g., *Gat*, 1996]. Because their concentration is sensitive to phase changes of water during its circulation, geographical and temporal variations of isotopic ratios emerge in land surface reservoirs such as rivers and groundwater. In order to understand, explain, and ultimately use observed variations in the reservoirs for assessing the hydrologic cycle, the relation between atmospheric processes and isotopic information in water vapor and precipitation has been intensively studied [e.g., *Craig and Gordon*, 1965; *Ehhalt*, 1974; *Jouzel*, 1986; *Gedzelman and Arnold*, 1994; *Webster and Heymsfield*, 2003; *Worden et al.*, 2007].

[3] Various empirical methods to explain the distribution of isotope ratio have been used since the classical ''isotopic effects'' was proposed (e.g., temperature effect [*Dansgaard*, 1964]). *Bowen and Revenaugh* [2003] showed that the monthly climatology precipitation isotope ratios can be reasonably well explained by a multivariate regression relationship with several meteorological and geographical variables. However, the accuracy of this multivariate relationship depends highly on the number of available observations, and much of the interannual variability is not captured by simple predictors (N. Buenning and D. Noone, Role of local and nonlocal processes in the seasonal cycle and interannual variability of the isotopic composition of precipitation deduced through observations and models, submitted to *Journal of Geophysical Research*, 2008). Since the observations are scarce, particularly for vapor isotopes and for both vapor and precipitation isotopes at time scales shorter than a month, the robustness of regression approaches still require further verification. In particular, simple regression models fail to capture the aspects of the isotope signal associated with atmospheric transport, and are thus ultimately limited. Perhaps more importantly, the physical mechanisms behind these empirical approaches need to be understood more explicitly.

[4] In contrast to observational studies, isotope-incorporated atmospheric general circulation models (AGCM) [*Joussaume et al.*, 1984; *Jouzel et al.*, 1987; *Hoffmann et al.*, 1998; *Mathieu et al.*, 2002; *Noone and Simmonds*, 2002; *Schmidt et al.*, 2005; *Lee et al.*, 2007] provide a more physical approach to understanding isotope distributions since they combine physical processes associated with the change in isotope ratio with the dynamic and moist thermodynamic processes of the atmosphere. These models simulate the three-dimensional structure of vapor isotope distribution with explicit consideration of complex phase changes of water associated with the moist physical processes in the global atmosphere. The resulting simulations show good agreement with climatological distribution of precipitation isotopes, but their temporal variability does

[1] Scripps Institution of Oceanography, University of California, La Jolla, California, USA.
[2] Institute of Industrial Science, University of Tokyo, Tokyo, Japan.
[3] Department of Atmospheric and Oceanic Sciences, and Cooperative Institute for Research in Environmental Sciences, University of Colorado at Boulder, Boulder, Colorado, USA.

Copyright 2008 by the American Geophysical Union.
0148-0227/08/2008JD010074$09.00

not agree well with the observations [*Hoffmann et al.*, 2000]. The reason for this poor isotope simulation is partly due to the inferior representation of atmospheric circulation by the AGCMs forced only by the observed sea surface temperature, and is also associated with the AGCMs' ability to simulate variability in the hydrologic cycle.

[5] *Yoshimura et al.* [2003, 2004] successfully reproduced the daily to interannual variations of precipitation isotopes over the globe using a simpler model in which the observed circulation was prescribed from atmospheric Reanalysis. They concluded that the isotopes can be used to evaluate the atmospheric moisture transport in models and that the isotopic AGCMs would be capable of simulating day-to-day isotopic variations in precipitation more accurately if the large-scale circulation fields are more accurately simulated. This finding also indicates that by constraining the isotopic fields the simulation of water vapor transport can be improved, but this issue leaves for future studies. Furthermore, vapor isotopes observed by satellites quantified the re-evaporation of tropical rainfall [*Worden et al.*, 2007], and the isotope simulations clarified that there is a need for evaporation of rain to remoisten the lower troposphere in AGCMs [*Noone*, 2003].

[6] Recently, *Yoshimura and Kanamitsu* [2008] used a spectral nudging technique for global downscaling of global Reanalysis. In this method, small-scale detail is generated by the high-resolution global model, whose large-scale circulations is constrained by the coarse resolution global atmospheric Reanalysis. The technique can be regarded as an economical alternative to computationally demanding high-resolution data assimilation. In this current study we apply the global spectral nudging technique not for a downscaling purpose, but for providing dynamical constraints to the water isotope circulations. It is expected that multidecadal and three dimensional distributions of isotopic species that are consistent with observed atmospheric circulation can be obtained. We used version of the Scripps global spectral model with water isotopes-incorporated (IsoGSM), which was newly developed from the up-to-date version of the Scripps Experimental Climate Prediction Center's (ECPC) GSM [*Kanamitsu et al.*, 2002a]. As an atmospheric analysis, the National Centers for Environmental Prediction (NCEP)/Department of Energy (DOE) Reanalysis 2 (R2) [*Kanamitsu et al.*, 2002b] was used to constrain the meteorology.

[7] This study has two main aims. The first is to make a long-term and three-dimensional data set of stable water isotopes, which is thermo-dynamically consistent with observed long and short-term atmospheric circulations. The results aid in understanding the mechanisms controlling of the global distributions and temporal variations of isotopes in a similar manner to that understanding atmospheric circulation on various time scales has benefited from Reanalysis products. The second aim is to make a reference isotopic variability analysis based on the model forced by observed atmospheric circulation. This analysis can be used to measure the a priori quality of the model performance for future studies involving the assimilation of isotopic data. This aim comes with an additional interest to establish the potential for improvement in the analysis of atmospheric circulation by the introduction of isotopes in a full data assimilation.

[8] Section 2 describes the new isotopic AGCM, the nudging method, and the simulation specification to make the isotopic data set. In section 3 the simulated isotope distribution is verified against observations and compared with other isotopic AGCMs. Improvements in the representations of the isotopic interannual variability are described in section 4. A summary and conclusions follow in section 5.

2. Method

2.1. Model Description

[9] Isotope processes were incorporated into the Scripps ECPC GSM in this study, hereafter IsoGSM. ECPC GSM was based on the medium range forecast model used at NCEP for making operational analysis and predictions [*Kanamitsu et al.*, 2002a]. The physics and dynamics of the model are mostly the same as those in the Reanalysis 2 project, but there have been updates associated with the use of a Relaxed Arakawa-Shubert deep convection scheme (RAS) [*Moorthi and Suarez*, 1992] and the Noah land surface model [*Ek et al.*, 2003]. As an operational weather forecast model, the basic performance of the NCEP GSM suites have been well documented [e.g., *Caplan et al.*, 1997; *Kanamitsu et al.*, 2002a] and have shown comparable performance in several global model intercomparison studies [e.g., *Kang et al.*, 2002].

[10] Gaseous forms of isotopic species (HDO and $H_2^{18}O$) were incorporated into the GSM as prognostic variables in addition to water vapor. The isotopic tracers are independently advected by the atmospheric circulations and transported by the subgrid-scale processes (convection and boundary layer turbulence). The specific components evolve differently during the condensation and evaporation associated with precipitation processes (convective precipitation and large-scale condensation) and surface and boundary layer processes, owing to the isotopic fractionation during the phase transitions.

[11] The equilibrium fractionation factors were taken from *Majoube* [1971a, 1971b]. Most fractionation at a phase transition can be assumed to occur at thermodynamic equilibrium, except for three particular cases; surface evaporation from open water [*Merlivat and Jouzel*, 1979]; condensation from vapor to ice in supersaturation conditions under -20°C [*Jouzel and Merlivat*, 1984]; and evaporation and isotopic exchange from liquid raindrop into unsaturated air [*Stewart*, 1975]. These are called kinetic fractionation, in which the difference of molecular diffusivities plays a key role when exchange occurs under conditions away from thermodynamic equilibrium. For consistency with other published isotopic AGCMs' results, we used the isotopic diffusivity coefficients measured by *Merlivat* [1978]. *Cappa et al.* [2003] measured slightly different values and produces a deuterium excess 3‰ systematically higher in the same conditions, but negligible on the variability [*Schmidt et al.*, 2005]. For the equilibrium fractionation, the Rayleigh distillation theory is applied for vapor condensation and evaporation during all the precipitation processes. These sets of isotopic parameterizations are commonly used among many AGCMs, following from the pioneering work of *Joussaume et al.* [1984].

Table 1. Summary of the Isotopic Parameterizations and the Spectral Nudging Technique

	Source/Description
Isotopic Parameterizations	
Equilibrium fractionation	*Majoube* [1971a, 1971b]
Molecular diffusivity	*Merlivat* [1978]
Ice crystal formation	*Jouzel and Merlivat* [1984]
Open water evaporation	*Merlivat and Jouzel* [1979]
Raindrop evaporation	*Stewart* [1975]
Surface isotopic reservoir	no fractionation, 50 mm bucket
Seawater	constant (δ^{18}O = δD = 0‰)
Forcings and Nudging Technique	
SST and sea ice	NCEP analysis
Circulation field forcing	Reanalysis 2 [*Kanamitsu et al.*, 2002b]
Nudging technique	*Yoshimura and Kanamitsu* [2008]
Nudging variables	U, V, and T
Nudging coefficient	0.9
Nudging scale	1000 km

[12] The isotopic fractionation during evaporation from surface water is expressed as

$$R_E = \alpha_{k\_mv}\frac{R_{sea}/\alpha_e - hR_a}{1-h}$$
$$\alpha_{k\_mv} = \begin{cases} 1 - A \cdots V < 7(\mathrm{m/s}) \\ 1 - (B \times V + C) \cdots V \geq 7(\mathrm{m/s}) \end{cases} \quad (1)$$

where R_E, R_{sea} and R_a indicate isotopic ratios of evaporative vapor, sea surface water, and ambient air, respectively, and α_e, V, and h are the equilibrium isotopic fractionation factor, surface wind speed, and relative humidity, respectively. Constants A, B, and C are 0.006, 0.000285, and 0.00082 for ^{18}O and 0.00528, 0.0002508, and 0.0007216 for D, as given by *Merlivat and Jouzel* [1979].

[13] For the condensation due to supersaturation, the following equations are used:

$$\alpha_{eff} = \alpha_{k\_jm}\alpha_e$$
$$\alpha_{k\_jm} = \frac{S}{\alpha_e(D/D')(S-1)+1}$$
$$S = \begin{cases} 1 \cdots T \geq -20^\circ C \\ 1 - 0.003T \cdots T < -20^\circ C. \end{cases} \quad (2)$$

where α_{eff} is an effective isotopic fractionation factor including the kinetic effect, α_e is the equilibrium isotope fractionation factor, D' and D are molecular diffusivities of isotopic vapor ($H_2^{18}O$ or HDO) and ordinary vapor (H_2O), T is air temperature in degree Celsius, and S is the oversaturation function parameterized by temperature. It was assumed that the liquid and ice phases coexist between -20°C to 0°C, and the effective fractionation factor is linearly interpolated between the two temperatures [*Ciais and Jouzel*, 1994].

[14] For evaporation and isotopic exchange from a falling droplet, the equations below are introduced according to *Stewart* [1975]:

$$m\frac{dR_r}{dm} = \beta(R_r - \gamma R_v)$$
$$\beta = \frac{1-\mu}{\mu}, \gamma = \frac{\alpha_e h}{1-\mu}, \mu = \alpha_e(D/D')^n(1-h) \quad (3)$$

where m is rain droplet volume, R_r and R_v are the isotopic ratio of rain droplet and ambient vapor, α_e is the equilibrium isotope fractionation factor, D' and D are molecular diffusivities of isotopic vapor and ordinary vapor, n is degree of freedom which is assumed 0.58 [*Gat*, 2000], and h is relative humidity. Equation (3) is integrated to yield

$$R_r = \varepsilon\left[(R_{r0} - \gamma R_{v0})(m/m_0)^\beta + \gamma R_{v0}\right] + (1-\varepsilon)R_{r0}$$
$$R_v = \left[q'_0 + \left(m'_0 - mR_r\right)\right]/q \quad (4)$$

where subscript 0 indicates original values before the isotopic effect, q' and m' denote vapor volume and rain droplet volume of the isotopic species, and ε is the fraction of the droplets reaching the isotopic equilibrium state. It is assumed that ε = 45% for convective clouds and ε = 95% for stratiform clouds, which captures the behavior that smaller drops more rapidly equilibrate [*Hoffmann et al.*, 2000].

[15] In convective clouds, entrained vapor at lower levels is lifted and eventually descends after losing its buoyancy. During its uplifting and condensation, formation of cloud liquid water and cloud ice take place, whereas evaporation from the particle takes place during its descent. Therefore convection plays a key role in the vertical mixing of isotopes in subgrid scales. In stratiform clouds, by contrast, the volume of large-scale condensation and evaporation is calculated downward from the top of the clouds. Isotopic ratios of these two different types of precipitation are saved as well as those of atmospheric vapor in each layer and evaporation flux.

[16] IsoGSM assumes no fractionation when water evapotranspires over land, which is a robust assumption on reasonably long time scales, even though there can be significant influences on the global isotopic cycle [e.g., *Yoshimura et al.*, 2006]. Separately from the proper NOAH land surface model, all precipitation is fully mixed into simple single bucket-type model for treatment of soil water isotopes, which provides storage of all water species, and consequently the isotope ratio of evapotranspiration can be assumed to be the same as stored values. All of these parameterizations in this section are summarized in Table 1.

2.2. Global Spectral Nudging Technique

[17] This study adopts the spectral nudging technique for a global simulation [*Yoshimura and Kanamitsu*, 2008]. Fourier series coefficients of zonal waves whose physical zonal scale is larger than the critical nudging scale L are nudged toward those of the analysis by the nudging weighting constant w defined as follows:

$$f_{(\lambda,\phi)} = \sum_{m=-M}^{m=M} A_{(m,\phi)}e^{im\lambda}$$
$$A_{(m,\phi)} = \begin{cases} A_{f(m,\phi)} & \left(|m| > \dfrac{2\pi r_E \cos\phi}{L}\right) \\ \dfrac{1}{w+1}\left(A_{f(m,\phi)} + wA_{a(m,\phi)}\right) & \left(|m| \leq \dfrac{2\pi r_E \cos\phi}{L}\right) \end{cases} \quad (5)$$

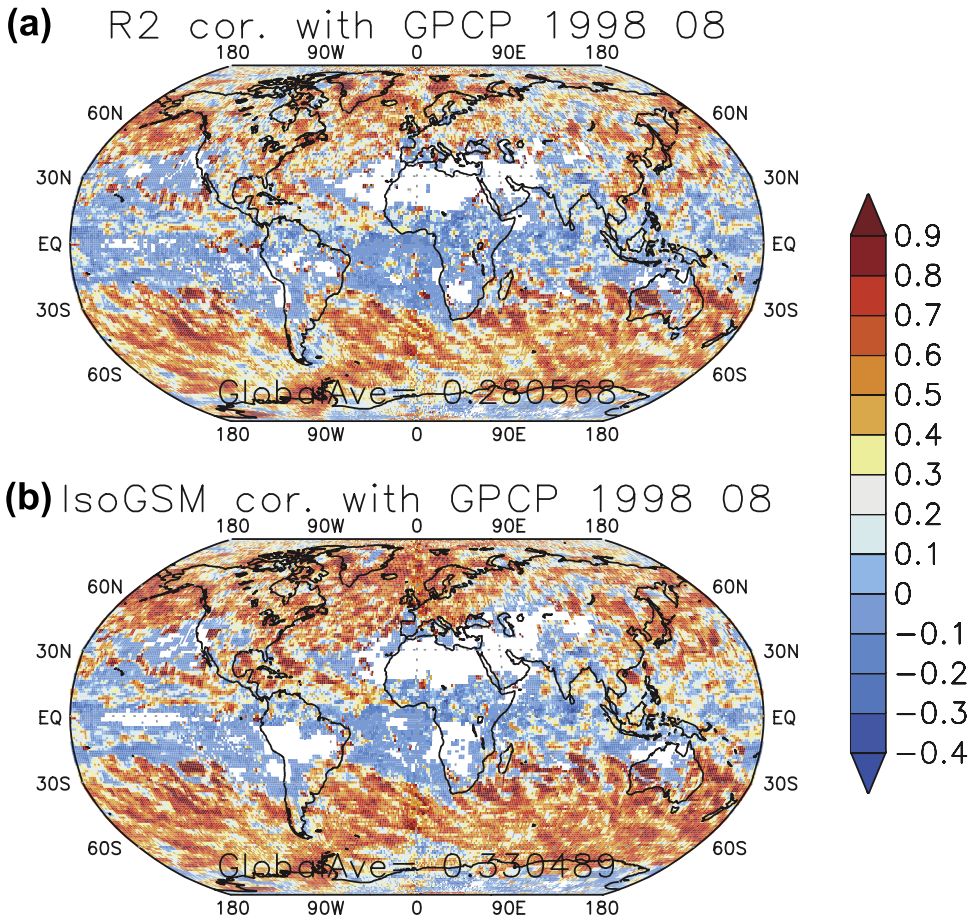

Figure 1. Global distribution of correlation coefficients in daily precipitation between GPCP and (a) NCEP/DOE Reanalysis and (b) IsoGSM in August 1998.

where f denotes a state model variable, A is the Fourier series coefficient, and the subscript $_f$ and $_a$ indicate forecast and analysis, respectively. λ, φ, r_E, m and M indicate longitude, latitude, radius of the earth, zonal wave number, and the truncation wave number, respectively. In this study, $w = 0.9$ and $L = 1000$ km were used and temperature, zonal and meridional wind components were nudged every time step toward 6-hourly R2 data at all 28 sigma-levels. This method only nudges zonal waves at each Gaussian latitude because the zonal spectral nudging is slightly more effective than the horizontally uniform-scale nudging owing to the heterogeneous characteristics of the large-scale atmosphere [*Yoshimura and Kanamitsu*, 2008]. Water vapor and the isotope species were not nudged, and were predicted using their conservation laws.

[18] A root mean square (RMS) difference of 500 hPa geopotential height provides a convenient summary measure of the fit between the nudged simulation and the R2 data. The RMS difference is typically 4–7 m averaged over all 6-hourly verification periods, which is well within the range of observation error of radiosondes indicating that the simulation faithfully reproduces the large-scale field of the Reanalysis. Figure 1 shows the global distributions of correlation in daily precipitation of the original R2 (Figure 1a) and the nudged experiment (Figure 1b) compared with Global Precipitation Climatology Project (GPCP) [*Huffman et al.*, 1997], in August 1998. The daily precipitation was slightly improved in the nudged experiment over entire globe mostly because of the updated physical processes described above, but the spatial distribution is very similar each other. These indicate that the nudging scheme without humidity can generate similar (even better) hydrologic cycle as R2. For more details of the result of the spectral nudging, see *Yoshimura and Kanamitsu* [2008].

2.3. Simulation Designs

[19] We chose T62 horizontal resolution (about 200 km) and 28 vertical sigma levels for isotope simulation, the same resolution as R2. After a spin-up period of about 10 years with the constant 1979 forcing, the simulation was run from 1979 to 2006, the period for which R2 data is available. The sea surface temperature and ice distribution used in R2 were used as lower boundary conditions. The monthly averaged precipitation isotope distributions from the simulation were compared with Global Network of Isotopes in Precipitation (GNIP) observations (International Atomic Energy Agency, http://isohis.iaea.org, 2001). Daily observation data over Thailand were taken from *Yoshimura et al.* [2003] for validation of the high-frequency variability. To show effectiveness of the nudging technique, the unnudged simulation results with the identical model are prepared, but only 2-year data are available owing to some resource

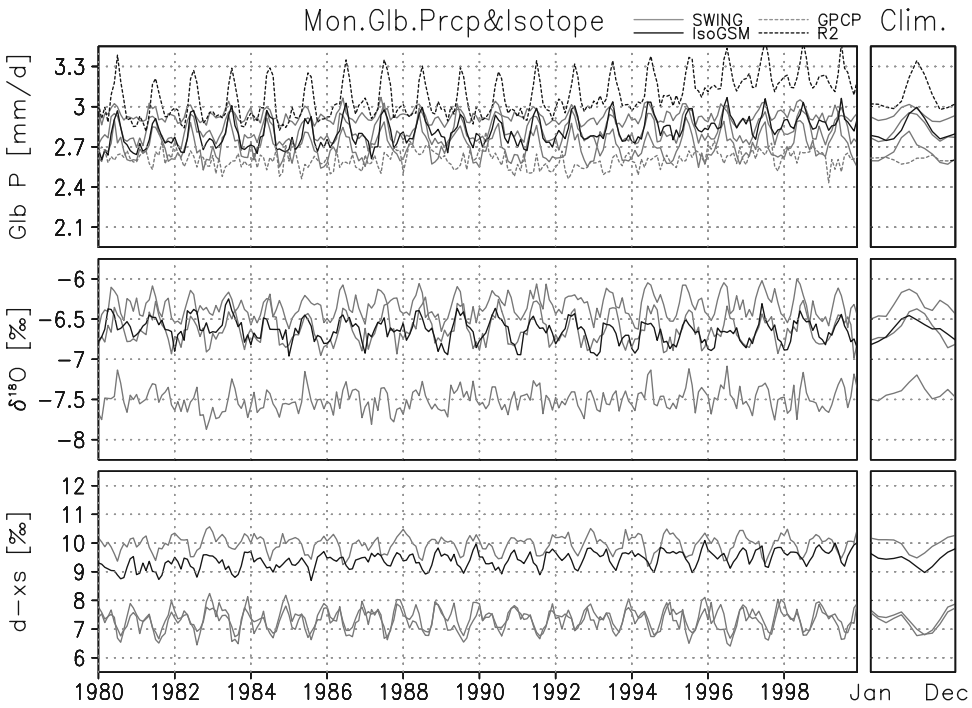

Figure 2. Monthly variation and climatology of global mean precipitation, δ^{18}O, and d-excess. Gray lines indicate ranges of three simulations by SWING member. Gray dashed, black dashed, and black solid lines show GPCP, R2, and IsoGSM, respectively.

problems. Therefore this study mainly uses the long-term simulation outputs from three other isotopic AGCMs archived by the Stable Water-Isotopes Intercomparison Group (SWING) [*Noone*, 2006]. This comparison should be valid for our purpose because the isotopic parameterization schemes in those models including IsoGSM are very similar each other. Hereafter the IsoGSM result designates that of the nudged simulation unless specified.

3. Results and Verification

3.1. Long-Term Trend of Isotopes in Global Precipitation

[20] Figure 2 presents the 20-year (1980–1999) time series and climatology of global monthly mean precipitation δ^{18}O and deuterium excess (d-excess; defined as δD-8*δ^{18}O). The simulated values from three isotopic SWING AGCMs are also shown. It is found that the globally averaged precipitation amount of the current simulation became systematically smaller than R2 but comparable to other models, and that a statistically significant trend in global precipitation (0.078 mm/day/10year) is detected in the nudged IsoGSM simulation. The former is probably because the humidity field was not nudged but the physical processes including convective precipitation were improved from the R2 model. The latter is because the simulation inherited the positive precipitation trend of R2 (as found in Figure 2), which is caused by the positive trend in the latent heat flux over oceans as a result of the positive trend in SST. The latest Reanalysis products by European Centre for Medium-Range Weather Forecasts (ECMWF), ECMWF 40-year Re-analysis (ERA40), and Japan Meteorological Agency, JRA25, also showed strong positive trends [*Chen and Bosilovich*, 2007], but some of them are known to be a result of the bias error of the satellite observations. Although both *Wentz et al.* [2007] and *Gu et al.* [2007] found a positive trend in oceanic global precipitation, the degree of the trend is much smaller (about one tenth) so that we are still not certain about credibility of the trend in Reanalysis. However, it is important to find that the current simulation captures the low-frequency features of the Reanalysis, indicating that the nudging technique performs as expected even in this time scale.

[21] Linear trends of the global precipitation δ^{18}O (−0.054‰/10year) and δD (−0.18‰/10year) are both slightly negative and a trend in d-excess (deuterium excess; defined as δD-8*δ^{18}O) (0.25‰/10 year) is significantly positive. These decreasing trends in δ^{18}O and δD and the increasing trend in d-excess are almost identical for evaporation and evaporative isotopes (figure not shown), indicating that the water cycle is in mass balance globally, and consequently there is almost no trend for total column vapor and its isotopes (Figure 3). *Craig and Gordon*'s [1965] formulation explains the inverse relation between long-term averaged evaporation rate and its isotopic ratios (Appendix A). The trends are statistically less significant for both δD and δ^{18}O where the interannual variability is large, but the trend is more significant in d-excess because of less the seasonal variation has smaller amplitude.

[22] Despite model differences, both the δ^{18}O and d-excess of our simulation are in the upper range of SWING members. Monthly climatology of global precipitation δ^{18}O and d-excess ranges from −7.0 to −6.5‰ and 8 to 10‰, respectively. Seasonality of δ^{18}O and d-excess resembles the pattern as that of precipitation indicating the seasonality is strongly influenced by precipitation total.

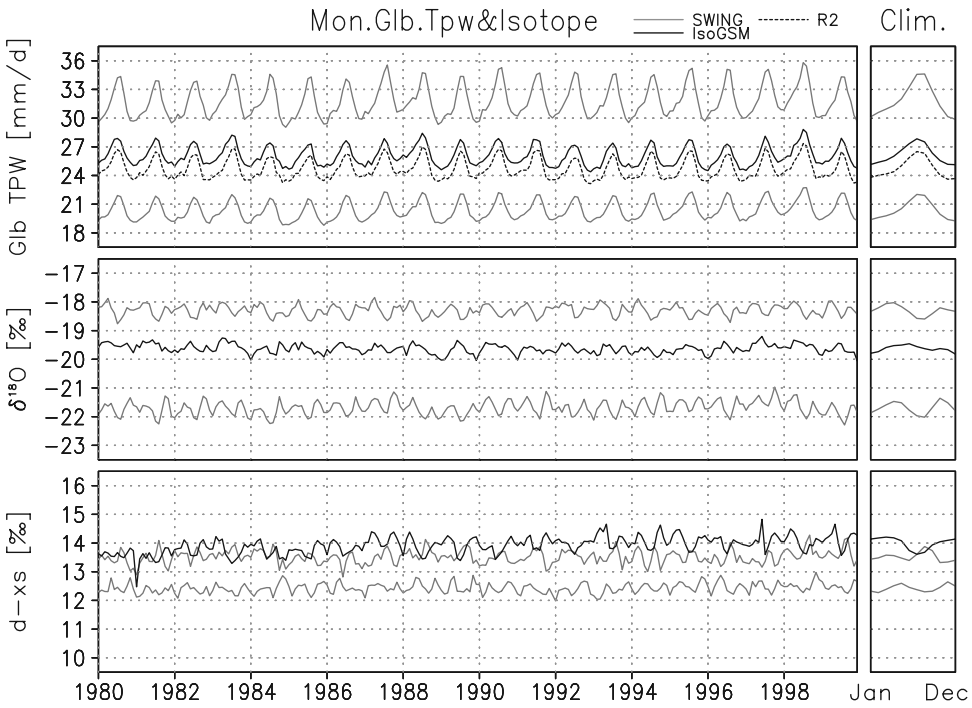

Figure 3. Same as Figure 2 but for total precipitable water. The results from MUGCM are excluded from gray SWING lines.

3.2. Climatology of Global Distribution of Isotopes

[23] Figure 4 shows annual climatology and difference between winter and summer (DJF-JJA) precipitation δ^{18}O for observation (GNIP), multimodel mean (SWING), and our simulations with and without nudging (IsoGSM_nudged and IsoGSM_unnudged). Note that the unnudged results are averages of only for 2 years (1998 and 2006). The nudged IsoGSM simulation agrees well with the observation for both annual and seasonal climatology as does the SWING multimodel data and the unnudged IsoGSM data.

[24] The biggest difference between SWING and IsoGSM lies over the plateau of Antarctica. As temperature decreases in JJA, precipitation δ^{18}O increases in our simulation. This is considered to be a deficiency in our model, which is caused by the numerical scheme used for moisture transport, and thus the error is associated with an extremely dry condition over the area during the winter (JJA) period, and the same problem noted in other studies [*Jouzel et al.*, 1987]. Fortunately, these erroneous isotopic ratios over extremely dry regions do not influence other areas because the mass of vapor is simply very small.

[25] Figure 5 evaluates the annual climatology and the winter-summer difference of δ^{18}O by comparing the nudged IsoGSM and SWING results with observations at all the GNIP sites. Correlation coefficients between this simulation and GNIP are 0.916 and 0.862 for annual δ^{18}O and winter-summer difference, respectively, whereas the same metrics show similar value ranges of 0.846∼0.884 and 0.750∼0.838, respectively, for the SWING members. This is due to the similarity of the isotopic parameterization schemes used in this model and the SWING models, and this also demonstrates common limitations of the current isotopic parameterization schemes.

[26] Figure 6 shows scatterplots similar to those of Figure 5, but for d-excess. The d-excess is particularly sensitive to kinetic processes in water surface and postcondensation processes, and it has more complex geographical distribution. The agreement of d-excess to observation is weaker than that of δ^{18}O. Correlations for annual means and winter-summer difference are 0.389 and 0.467 in IsoGSM, and these are in ranges of 0.409∼0.552 and 0.052∼0.524 for the three SWING simulations. In terms of agreement of d-excess with observation, this IsoGSM simulation does not show clear advantages over SWING simulations, even though it is associated with the true meteorology.

3.3. Daily to Interannual Variations Over Specific Locations

3.3.1. Daily Variations of δ^{18}O in Precipitation Over Thailand

[27] The advantage of an experiment using observed atmospheric circulation is that the analysis provides wide ranges of time scales, and allows us to compare diurnal through interannual variability with real observations. Figure 7 compares daily precipitation isotopic ratios at three sites over Thailand. The day-to-day variation was well captured in the IsoGSM simulation. In all of the SWING simulations, this type of comparison is not possible since each model generates its own meteorology, and thus there is no direct counterpart of observations. This analysis confirms the results of *Yoshimura et al.* [2003] (hereafter Y03), who found that large-scale moisture transport is the main control of the daily isotopic variations.

[28] Y03 used the ''well-mixed'' assumption in a vertical column and only allowed the equilibrium fractionation during precipitation. On the contrary, the current study incorporated more detailed vertically varying aspects of processes controlling isotopic fractionation during precipi-

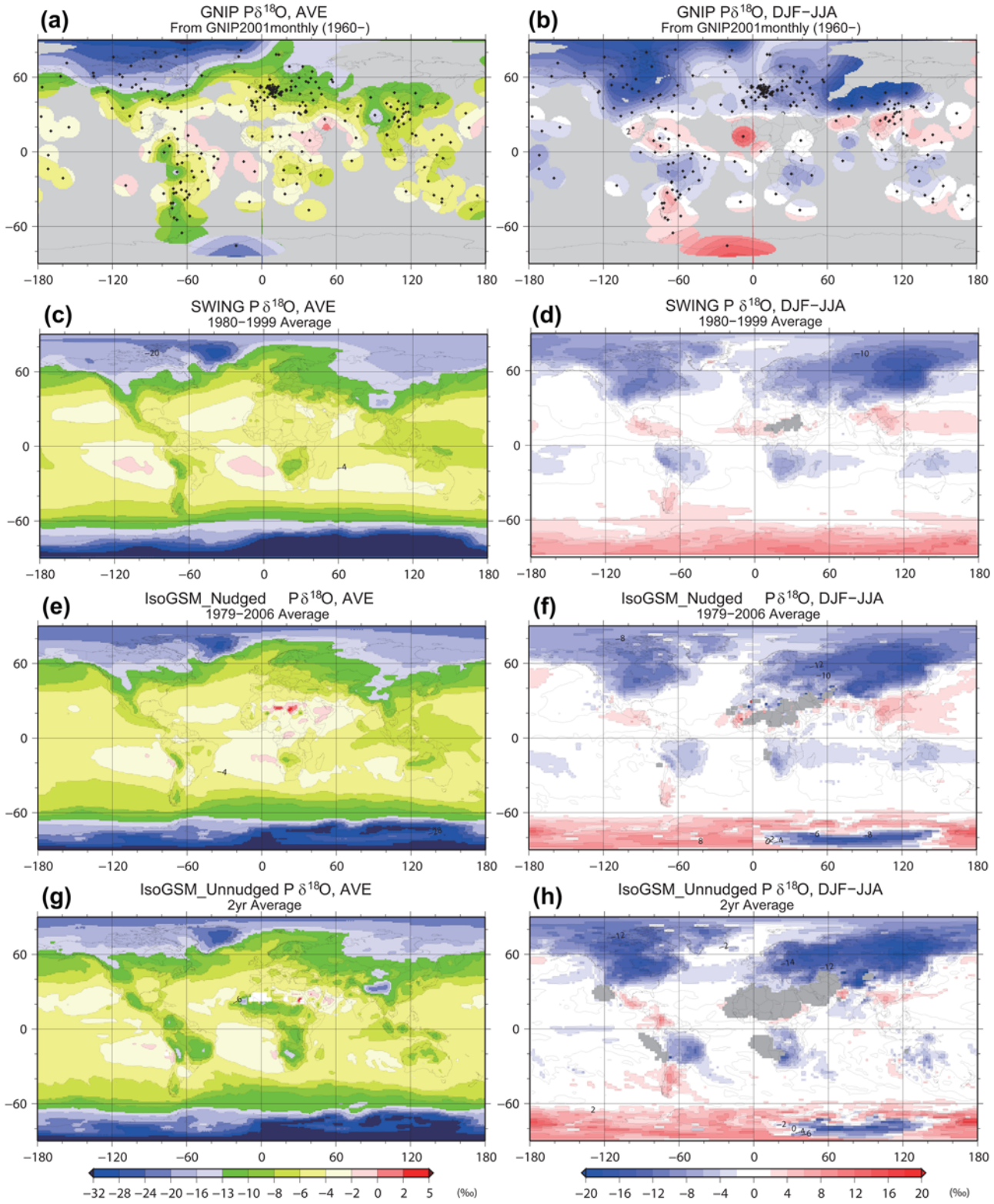

Figure 4. (a, c, e, and g) Annual average and (b, d, f, and h) seasonal difference of precipitation isotope ratio (δ^{18}O) by GNIP observations (Figures 4a and 4b), SWING multimodel means (Figures 4c and 4d), the nudged IsoGSM simulation (Figures 4e and 4f), and the unnudged IsoGSM simulation (Figures 4g and 4h).

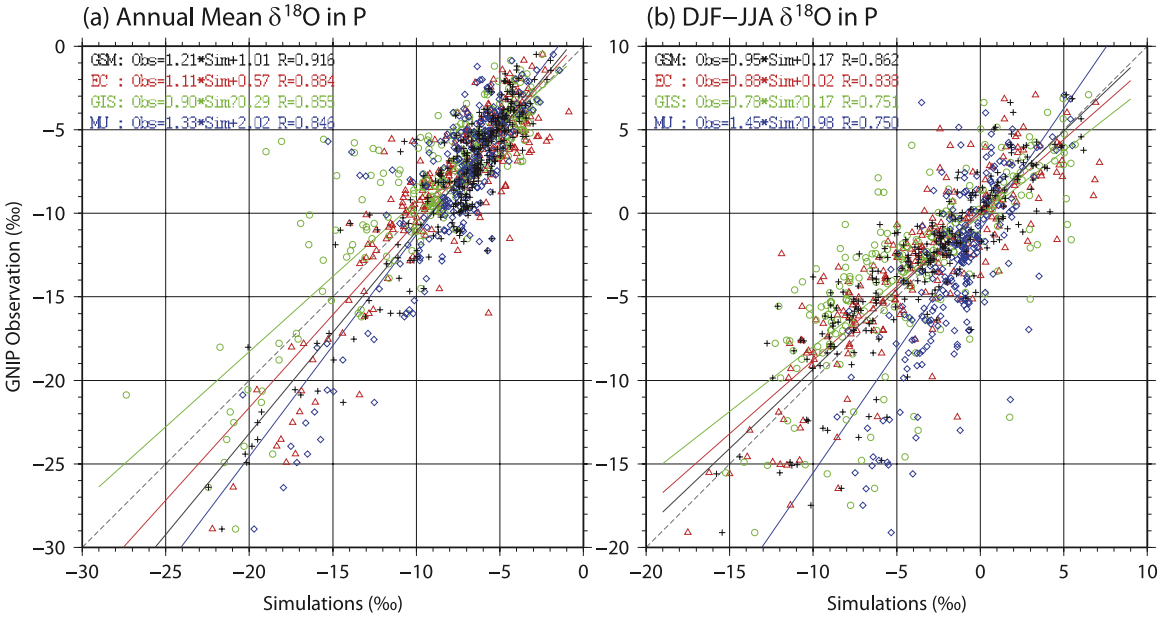

Figure 5. Scatterplots of direct comparison of (a) annual mean and (b) seasonal departure of $\delta^{18}O$ in precipitation for both IsoGSM (black crosses) and the three SWING members (red, green, and blue for ECHAM, GISS, and MUGCM, respectively).

tation without the well-mixed assumption. In these regards, the IsoGSM simulation should be superior to Y03 in terms of physical processes, but the correlation coefficients of the isotopic ratio between analysis and observation were 0.33 to 0.66, which were not as good as 0.48 to 0.77 in Y03 (as seen by gray lines in Figure 7).

[29] There seem to be two main reasons for this inferior performance: (1) greater potential for errors in the more complex set of moist processes incorporated into IsoGSM, and thus captured by the isotopes, and/or (2) accuracy of model produced precipitation. Y03 used observed GPCP precipitation instead of Reanalysis precipitation and is likely a key reason for their increased simulation performance. It is known that accuracy of daily precipitation amount in Reanalysis in low latitudinal regions is relatively poor owing to difficulties in reproducing convective precipitation in the forecast model [e.g., *Kalnay et al.*, 1996]. This was also true in the nudged IsoGSM simulation, having low JJA daily precipitation correlations of 0.2∼0.3 in average over the Indochina peninsula region between Reanalysis and GPCP (see Figure 1a for precipitation in August 1998). This error is thus inherited in the isotope simulation, resulting in lower correlations (see Figure 1b). As such the isotope results expose this shortcoming in the underly-

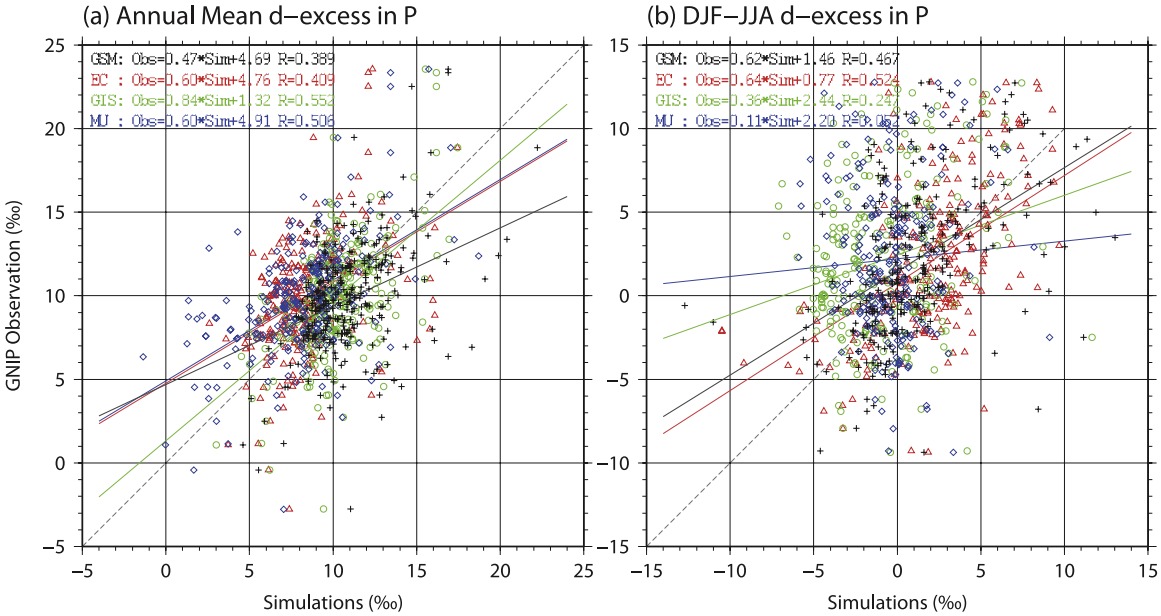

Figure 6. Same as Figure 5, but for d-excess.

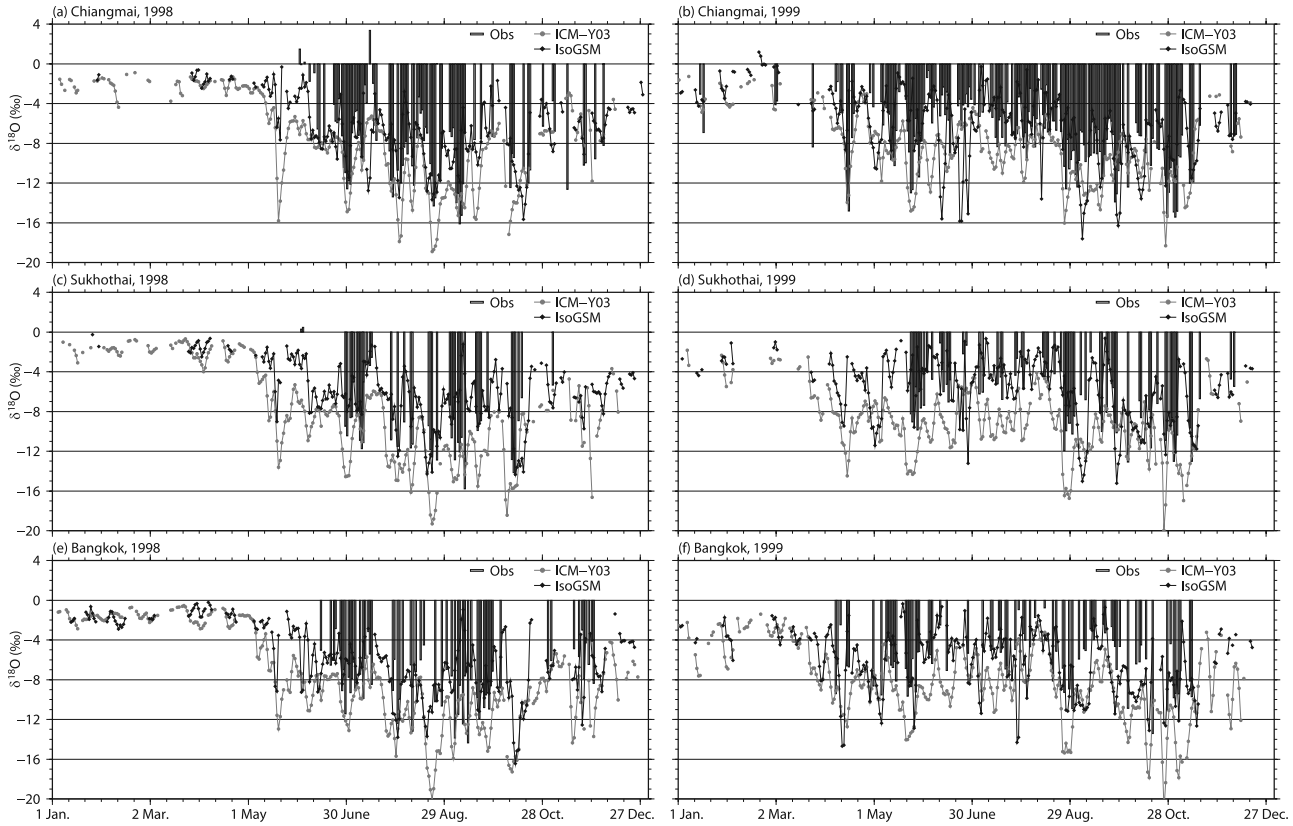

Figure 7. Daily variations of precipitation δ^{18}O at (a and b) Chiangmai, (c and d) Sukhothai, and (e and f) Bangkok in Thailand, 1998 (Figures 7a, 7c, and 7e) and 1999 (Figures 7b, 7d, and 7f). The bars indicate observations at three sites, and the black lines indicate IsoGSM simulations. Gray lines are the ICM results taken from *Yoshimura et al.* [2003, Figure 13].

ing hydrological simulation, and identify a need to further improve the convection parameterization in the model. Alternatively, the results expose that observed precipitation might need to be used as an additional constraint on the hydrologic cycle to further improve the isotope simulations.

3.3.2. Interannual Variations of Monthly Anomaly δ^{18}O

[30] Figure 8 shows variations in monthly anomaly of precipitation δ^{18}O at Vienna and Bangkok. The climatology of precipitation isotopes were reasonably well-simulated by all isotopic AGCMs, therefore an additional value of the new data set should lie in the reproduction of the interannual variability. It is comforting to find that both at Vienna and Bangkok the interannual variations are reproduced only by the IsoGSM simulation.

[31] Table 2 shows the number of GNIP sites where simulations credibly reproduced (positive correlation exceeding 90% significance) the δ^{18}O in monthly precipitation and their monthly anomalies in different latitudinal regions. It clearly shows that the IsoGSM simulation had better accuracy in the monthly variability over all regions compared with the three models in SWING. Furthermore, the IsoGSM simulation showed drastic improvements for the interannual variability of the monthly anomaly of precipitation δ^{18}O. The largest improvement exists in midlatitudes to high latitudes in the NH (northward of 30N), where SWING showed an agreement of 9% with the observation sites at best, whereas this study showed an astonishing 72% agreement. On the other hand, over the Tropics (30S–30N) and the SH (southward of 30S), the improvement was less than that of the NH; from 18% to 48% and from 10% to 41%, respectively. The reason for the difference in the improvements will be discussed in section 4.

[32] This overall success was primarily due to the use of observed atmospheric circulation, while the other models were inferior owing to their inability to simulate the interannual variation of atmospheric circulation when forced only by SST (and sea ice). It should be emphasized that this result does not imply superiority of the isotopic parameterization used in the current model nor improvement in other dynamical and physical processes, but it does imply the importance of atmospheric circulation.

4. Interannual Variability

[33] Above it was found that the monthly anomalies were clearly better reproduced owing to the nudging of observed atmospheric circulation. We are thus now well placed to investigate the degree to which the interannual variability of the isotopes in the observations and the simulations with and without nudging is associated with organized patterns of variability, such as ENSO and Annular modes.

4.1. ENSO Mode

[34] Figure 9 shows global distributions of the correlation between monthly anomaly δ^{18}O and the multivariate ENSO

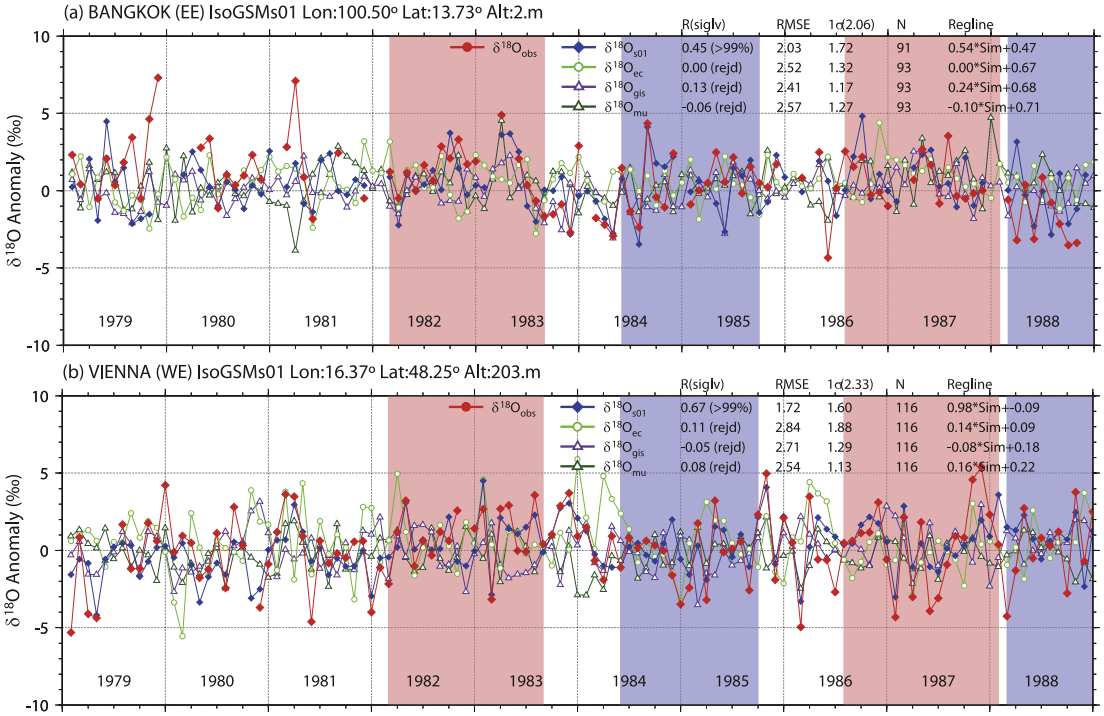

Figure 8. Monthly variation of precipitation $\delta^{18}O$ anomaly at (a) Bangkok and (b) Vienna. Red lines are GNIP, blue lines are IsoGSM, and other lines are from the three SWING members. Light pink and blue shades indicate El Niño and La Niña periods, respectively, derived by the NINO3 index.

index (MEI) [*Wolter and Timlin*, 1998]. The observation showed significant positive correlation over Southeast Asia, the maritime continents, Eastern Europe, and the tropical Amazon. Even though the data are sparse, in the middle of both the Pacific and Atlantic Oceans, there are also positively correlated sites. In the SWING simulations (Figures 9c–9e), negatively correlated regions over the equatorial eastern Pacific Ocean are apparent, which are surrounded by positively correlated regions over the western Pacific and the maritime continents. There are also significantly positive correlations in the Amazon and in northwestern Canada.

[35] These geographical patterns of anomaly correlation between isotope variation with the ENSO index are very similar in the IsoGSM simulation (Figure 9b), but the signals are slightly stronger in general. Those correlations agree well with those of GNIP, except for the sites in western Eurasia, including three sites in Europe. The ENSO signal, which is driven by SST variability, was prescribed in the SWING models and faithfully reproduced in our simulation owing to the spectral nudging (inherited from Reanalysis 2). Hence the signals in the monthly anomalies in precipitation $\delta^{18}O$ were also captured well in all SWING models and in the IsoGSM simulation, particularly over the Pacific Ocean. Therefore there is little gain by the nudging of the observed atmospheric circulation in this respect. It should be noted however that IsoGSM shows better agreement with the observations over Southeast Asia, and indeed shows some evidence for positive correlations over Europe that do not occur in the SWING models, but are found in observations.

Table 2. Number of GNIP Sites Where Monthly $\delta^{18}O$ and Monthly Anomaly of $\delta^{18}O$ Are > 95% Significantly Correlated With Each SWING and IsoGSM Simulation[a]

	Comparison with GNIP for 1980–1999			
	ECHAM	GISS-E	MUGCM	IsoGSM
		Correlation		
NH (210)	147	171 (81%)	116	174 (83%)
Tropics (142)	68	82 (58%)	46	96 (68%)
SH (37)	22 (60%)	18	16	25 (68%)
		Anomaly Correlation		
NH (146)	13 (9%)	12	6	114 (78%)
Tropics (67)	9	12 (18%)	6	32 (48%)
SH (29)	1	3 (10%)	1	12 (41%)

[a]The globe is divided by three regions: NH (northward of 30N), Tropics (30S–30N), and SH (southward of 30S). Total numbers of sites available for each comparison are shown in parentheses next to the region name. The percentages to the total available sites are also shown in parentheses, but only the best is shown for the SWING member.

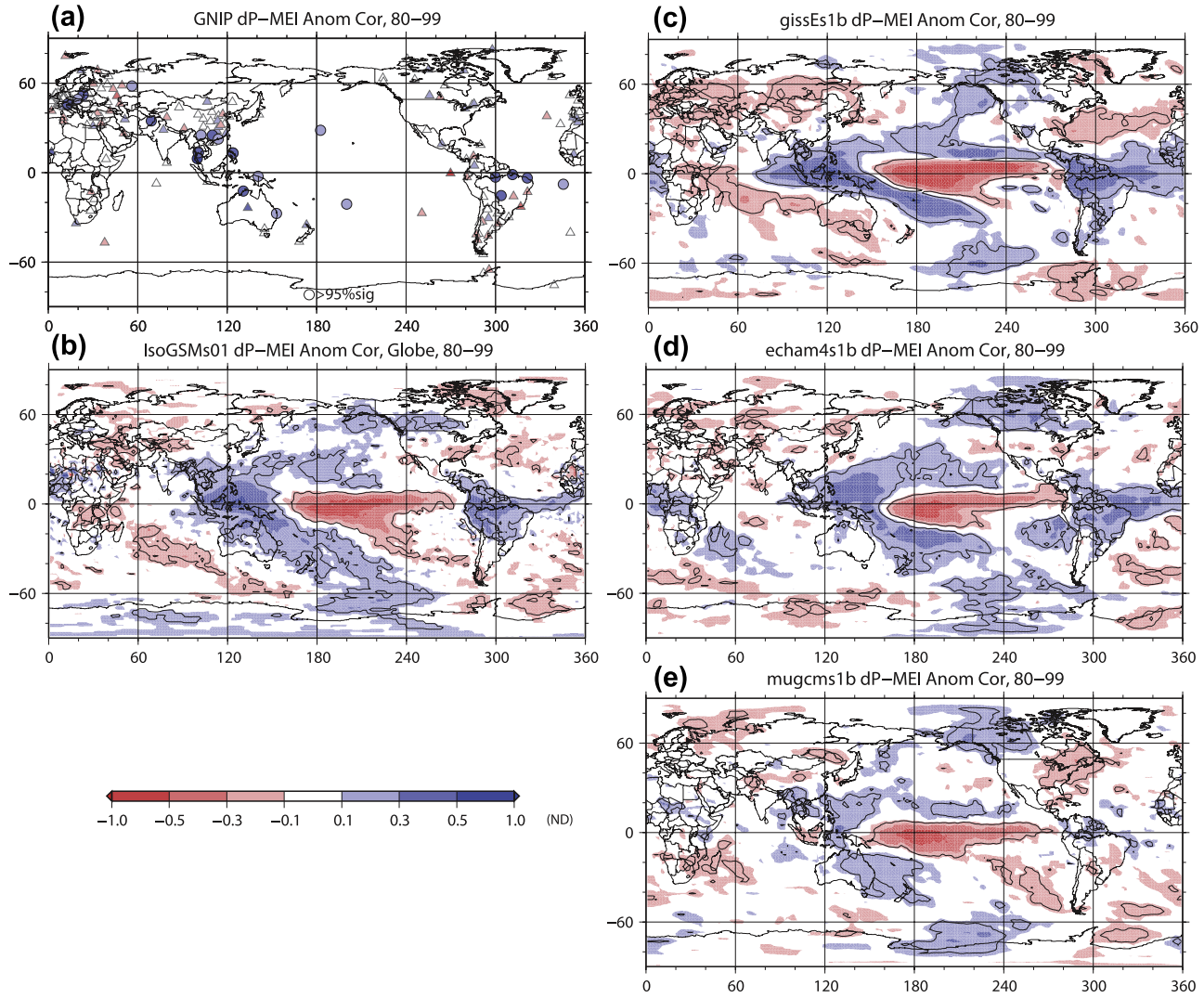

Figure 9. Distribution of correlation coefficients between monthly anomaly of precipitation $\delta^{18}O$ and MEI for (a) GNIP, (b) SWING multimodel mean, and (c) IsoGSM. In Figure 9a, correlations with significance levels greater than 95% are indicated by circles and other sites are shown by triangles. In Figures 9b and 9c, correlations with significance levels greater than 99% are contained by black solid lines.

4.2. AO Mode

[36] The Arctic Oscillation (AO) is one of the most dominant atmospheric patterns in the NH. The long-term trend is found to be closely related to this mode [*Thompson and Wallace*, 2000]. The monthly AO index is defined as the leading Empirical Orthogonal Function (EOF) to the monthly mean 1000-hPa height (or sea level pressure) anomalies poleward of 20° latitude for the Northern Hemisphere. Figure 10 shows the observed monthly AO index calculated by NCEP Climate Prediction Center (CPC) (http://www.cpc.ncep.noaa.gov/products/precip/CWlink/daily_ao_index/ao.shtml, 2008) and the same indices calculated by the current and the SWING simulations. Because of the nudging of the dynamical fields, the IsoGSM AO is very similar to the observation (R = 0.83), whereas the SWING members created their own variability (R = 0.06∼0.25). More importantly, the leading frequency of the CPC and IsoGSM lies in a range of 2∼3 years, whereas shorter frequency is dominant in the SWING simulations (several months to 2 years), indicating that the simulations forced by only SST had difficulty to reproduce the oscillation frequency.

[37] There have been studies that have shown the AO to be linked to strong regional isotopic signals [*Welker et al.*, 2005; *Rimbu et al.*, 2006; *Schneider and Noone*, 2007]. Figure 11 shows NH distributions of the correlation between monthly anomaly $\delta^{18}O$ and their own monthly AO indices. The correlation between GNIP observation and CPC's AO index (Figure 11a) indicates that many sites in Europe have significant positive correlations. Some negative correlations are seen over northern Canada, Greenland, and Iceland even though the signs are not statistically significant. There are also nonsignificant positive (negative) correlations in northeastern (southeastern) China.

[38] The IsoGSM simulation (Figure 11b) and the SWING simulations (Figures 11c–11e) have somewhat

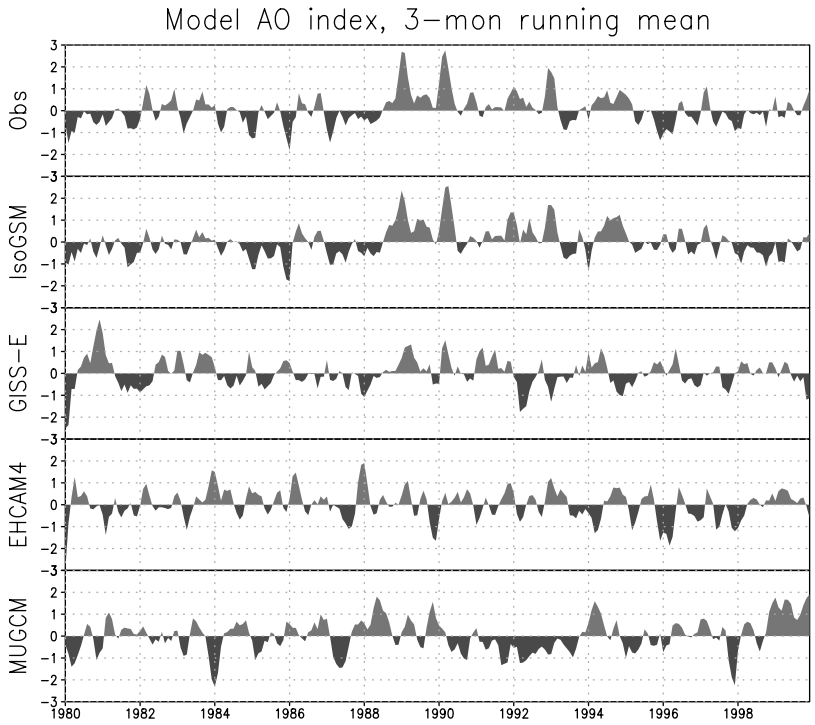

Figure 10. Monthly Arctic Oscillation indices of observation and models (IsoGSM and three SWING members). Three-month running mean values with adjacent months are shown.

similar distribution of signals in precipitation isotopes derived from AO. The significantly positive signal is commonly covering all of Europe, which agrees with the observations. The negative signals covering the Arctic Archipelago/Greenland are also common in the all simulations, which agree with observations but the observed signals are statistically less significant. Though the simulation period is very short and therefore the statistical significance is much weaker than the others, the similar signals are detectable in the unnudged IsoGSM simulation result (Figure 11f). Such spatial distributions were also seen in the coupled isotopic model integration [*Schmidt et al.*, 2007]. However, all SWING simulations have strong positive signals over northeastern part of the North America, but such signals are not apparent in the observation and the nudged IsoGSM simulation. Moreover, the observed negative correlations in southeastern China are simulated in IsoGSM and ECHAM4 only.

[39] Unlike to the ENSO signal, there are substantial improvements to the ability to capture the real AO signal by nudging. It is known that the AO signal is more difficult to reproduce than the ENSO signal in current AGCMs forced only by SST, since the AO is more likely to be forced internally by dynamics as compared to the ENSO mode which is externally forced (by SST) [*Feldstein*, 2000, 2002]. Therefore, it can be concluded that the atmospheric forcing in R2, which already had the realistic AO signal, made the monthly isotopic variability more realistic over midlatitudes to high latitudes in the NH, especially Europe, while this is not the case in the SWING simulations because the SST forcing along is not enough to reproduce a reliable AO history.

[40] These findings suggest that if one requires a faithful reproduction of the history of interannual variability in isotopic composition, one also needs to reproduce the atmospheric circulation with high fidelity. The findings also suggest, however, that the use of isotope observation from precipitation and/or ice cores, for example, may be used to obtain information on internal interannual modes and on making consistent analysis of atmospheric circulation.

5. Summary and Conclusions

[41] In this study, we produced a multidecadal and globally three-dimensional stable water isotope data set. This was accomplished by introducing the isotope fractionation process into the Scripps ECPC global spectral model, namely IsoGSM, and applying spectral nudging toward the meteorology captured by the NCEP/DOE Reanalysis. This procedure mimics the isotope distribution expected from a tracer simulation tied to meteorological data assimilation, and produces geographical distributions of isotopes more consistent with observed atmospheric circulation than those simulated with AGCMs forced only by observed SST. Even though this method did not directly assimilate the isotopic species observation, it can be regarded as a good proxy for ''Isotope Reanalysis,'' until isotope data assimilation becomes possible. An important advantage of this procedure is that the analysis provides more realistic isotope variation for a wide range of time scales from diurnal to interannual. Comparisons with limited station observations and global simulation results from other isotopic AGCM simulations showed that the current simulation agreed better with observations in those time scales. Of particular note, we find:

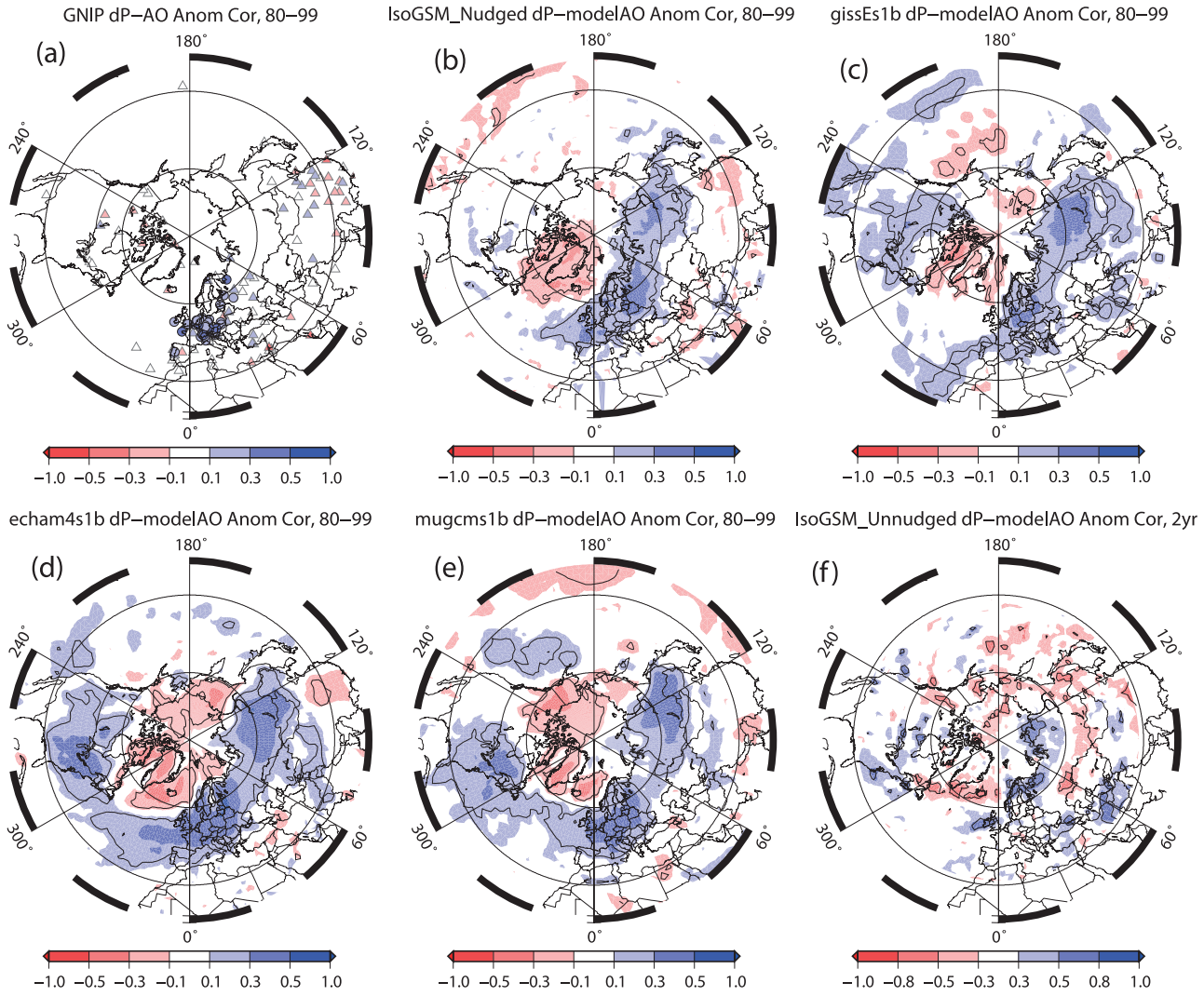

Figure 11. Same as Figure 10, but for correlation with the monthly AO over the NH. The correlation of the unnudged IsoGSM simulation is additionally shown in Figure 11f. The AO index is calculated from each model's sea level pressure. Note that a different color bar scale is used in the unnudged IsoGSM (Figure 11f) because the simulation period is shorter than the others.

[42] 1. Annual climatology and seasonal departure (DJF-JJA) of precipitation $\delta^{18}O$ agreed well with the observation data with a correlation of 0.92 and 0.86, respectively, all slightly better than those of the previous multimodel mean.

[43] 2. Annual climatology and winter-summer difference of precipitation d-excess were found to agree less well with observations than $\delta^{18}O$. The correlations with the observation were 0.39 and 0.47 for annual mean and seasonal difference, respectively. This is likely associated with the specific physics in the present model rather than a shortcoming of the nudging approach.

[44] 3. The accuracy of simulated daily precipitation $\delta^{18}O$ in terms of correlations with observation ranges from 0.33 to 0.66 for three sites during the 2 years for which the observations are available, but were consistently inferior to those simulated by a simpler two dimensional model by *Yoshimura et al.* [2003]. The reasons are considered to be due to (1) errors in the three dimensional isotopic process and/or (2) low accuracy of model produced precipitation.

[45] 4. The comparison of the fit of the simulated monthly precipitation $\delta^{18}O$ in this study and three SWING model simulations over about 390 GNIP sites revealed that the IsoGSM simulation is most accurate in representing the monthly variations. Much more apparent improvements were found in monthly anomaly variability: The largest improvement exists in the NH (northward of 30N) where "well-simulated" sites increased from 9% to 72%. Over the Tropics (30S–30N) and the SH (southward of 30S), the improvements were from 18% to 48% and from 10% to 41%, respectively.

[46] 5. In addition to the reasonable reproduction of correlation pattern between monthly anomaly $\delta^{18}O$ and the multivariate ENSO index, as in other models, the current approach reproduced the Arctic Oscillation much more correctly. This made the monthly isotopic variability more realistic over midlatitudes to high latitudes in the NH, especially Europe.

[47] The spatiotemporally interpolated isotope data which are consistent with Reanalysis meteorological variables are useful in at least two aspects; as boundary and initial conditions for isotopic regional model simulations [e.g., *Sturm et al.*, 2005], and for comparison and further analyses of in situ and short-term isotopic observations [e.g., *Fudeyasu et al.*, 2008; *Uemura et al.*, 2008], which are not routinely conducted.

[48] The improvement of isotope simulation in this study confirmed that the atmospheric circulation is important in determining its variability characteristics. This also implies that there is potential in using isotopic observation to obtain more accurate analysis of water transport via assimilation of isotopic data. Specific opportunities arise in assimilating, for instance, satellite observations of the isotopic composition of water vapor to constrain the contemporary water cycle, and the use of small amounts of data from ice core records to constrain simulations of glacial periods and other historical climates.

Appendix A: Inverse Proportion Between Evaporation Flux and Its Isotopic Ratio

[49] From *Craig and Gordon*'s [1965] equation, the isotopic ratio of evaporative flux, R_E, is expressed in terms of relative humidity, h, as follows:

$$R_E = \alpha_k \frac{R_{sea}/\alpha_e - hR_a}{1-h}$$

where R_{sea} and R_a are the isotope ratios of seawater and atmospheric vapor, respectively, α_k and α_e are kinetic and equilibrium fractionation factors. A calculation for evaporation flux, E, can be simplified as $E = ke_s(1-h)$, where k is an energy exchange factor, and e_s is the saturation vapor pressure. Therefore, the following equation with an inverse proportion between E and R_E can be introduced:

$$R_E = ke_s\alpha_k(R_{sea}/\alpha_e - R_a)\frac{1}{E} + \alpha_k R_a$$

[50] **Acknowledgments.** Part of this research was funded by the Japan Society for the Promotion of Science Postdoctoral Fellowships for Research Abroad. We would like to thank J. Roads for his constructive comments and C. Papadopoulos for her technical help with computational resources. This study was also partially supported by NSC 95-211-M133-001-AP4, NOAA NA17RJ1231, and JSPS (S)19106008. The views expressed herein are those of the authors and do not necessarily reflect the views of NOAA. We also thank Diane Boomer for closely proofreading the manuscript. All the data are open to public. Please visit http://meteora.ucsd.edu/~kyoshimura/IsoGSM1 for instructions.

References

Bowen, G. J., and J. Revenaugh (2003), Interpolating the isotopic composition of modern meteoric precipitation, *Water Resour. Res.*, *39*(10), 1299, doi:10.1029/2003WR002086.

Caplan, P., J. Derber, W. Gemmill, S. Y. Hong, H. L. Pan, and D. Parrish (1997), Changes to the 1995 NCEP operational medium-range forecast model analysis-forecast system, *Weather Forecasting*, *12*(3), 581–594.

Cappa, C. D., M. B. Hendricks, D. J. DePaolo, and R. C. Cohen (2003), Isotopic fractionation of water during evaporation, *J. Geophys. Res.*, *108*(D16), 4525, doi:10.1029/2003JD003597.

Chen, J., and M. G. Bosilovich (2007), Hydrological variability and trends in global reanalyses, Abstract JP4.4 presented at 19th Conference on Climate Variability and Change, Am. Meteorol. Soc., San Antonio, Tex.

Ciais, P., and J. Jouzel (1994), Deuterium and oxygen 18 in precipitation: Isotropic model, including mixed cloud processes, *J. Geophys. Res.*, *99*(D8), 16,793–16,803.

Craig, H., and L. Gordon (1965), Deuterium and oxygen-18 variations in the ocean and the marine atmosphere, in *Stable Isotopes in Oceanographic Studies and Paleotemperatures*, edited by E. Tongiorgi, pp. 9–130, Cons. Naz. delle Ric. Lab. di Geol. Nucl., Spoleto, Italy.

Dansgaard, W. (1964), Stable isotopes in precipitation, *Tellus*, *16*, 436–468.

Ehhalt, D. H. (1974), Vertical profiles of HTO, HDO and H2O in the troposphere, *Tech. Rep. NCAR-TN/STR-100*, Natl. Cent. for Atmos. Res., Boulder, Colo.

Ek, M. B., K. E. Mitchell, Y. Lin, E. Rogers, P. Grunmann, V. Koren, G. Gayno, and J. D. Tarpley (2003), Implementation of Noah land surface model advances in the National Centers for Environmental Prediction operational mesoscale Eta model, *J. Geophys. Res.*, *108*(D22), 8851, doi:10.1029/2002JD003296.

Feldstein, S. B. (2000), The timescale, power spectra, and climate noise properties of teleconnection patterns, *J. Clim.*, *13*, 4430–4440, doi:10.1175/1520-0442(2000)013<4430:TTPSAC>2.0.CO;2.

Feldstein, S. B. (2002), The recent trend and variance increase of the annular mode, *J. Clim.*, *15*, 88–94, doi:10.1175/1520-0442(2002)015<0088:TRTAVI>2.0.CO;2.

Fudeyasu, H., K. Ichiyanagi, A. Sugimoto, K. Yoshimura, A. Ueta, M. D. Yamanaka, and K. Ozawa (2008), Isotope ratios of precipitation and water vapor observed in Typhoon Shanshan, *J. Geophys. Res.*, *113*, D12113, doi:10.1029/2007JD009313.

Gat, J. R. (1996), Oxygen and hydrogen isotopes in the hydrologic cycle, *Annu. Rev. Earth Planet. Sci.*, *24*, 225–262, doi:10.1146/annurev.earth.24.1.225.

Gat, J. R. (2000), Atmospheric water balance-The isotopic perspective, *Hydrol. Process.*, *14*, 1357–1369, doi:10.1002/1099-1085(20000615)14:8<1357::AID-HYP986>3.0.CO;2-7.

Gedzelman, S. D., and R. Arnold (1994), Modeling the isotopic composition of precipitation, *J. Geophys. Res.*, *99*(D5), 10,455–10,471, doi:10.1029/93JD03518.

Gu, G., R. F. Adler, G. J. Huffman, and S. Curtis (2007), Tropical rainfall variability of interannual-to-interdecadal and longer time scales derived from the GPCP monthly product, *J. Clim.*, *20*, 4033–4046, doi:10.1175/JCLI4227.1.

Hoffmann, G., M. Werner, and M. Heimann (1998), Water isotope module of the ECHAM atmospheric general circulation model: A study on timescales from days to several years, *J. Geophys. Res.*, *103*(D14), 16,871–16,896, doi:10.1029/98JD00423.

Hoffmann, G., J. Jouzel, and V. Masson (2000), Stable water isotopes in atmospheric general circulation models, *Hydrol. Process.*, *14*, 1385–1406, doi:10.1002/1099-1085(20000615)14:8<1385::AID-HYP989>3.0.CO;2-1.

Huffman, G. J., R. F. Adler, P. Arkin, A. Chang, R. Ferraro, A. Gruber, J. Janowiak, A. McNab, B. Rudolf, and U. Schneider (1997), The global precipitation climatology project (GPCP) version 1 dataset, *Bull. Am. Meteorol. Soc.*, *78*, 5–20, doi:10.1175/1520-0477(1997)078<0005:TGPCPG>2.0.CO;2.

Joussaume, S., R. Sadourny, and J. Jouzel (1984), A general circulation model of water isotope cycles in the atmosphere, *Nature*, *311*, 24–29, doi:10.1038/311024a0.

Jouzel, J. (1986), Isotopes in cloud physics: Multiphase and multistage condensation processes, in *Handbook of Environmental Isotope Geochemistry*, vol. 2, edited by P. Fritz and J. C. Fontes, pp. 61–112, Elsevier, New York.

Jouzel, J., and L. Merlivat (1984), Deuterium and oxygen 18 in precipitation: Modeling of the isotopic effects during snow formation, *J. Geophys. Res.*, *89*, 11,749–11,757, doi:10.1029/JD089iD07p11749.

Jouzel, J., G. L. Russell, R. J. Suozzo, R. D. Koster, J. W. C. White, and W. S. Broecker (1987), Simulations of the HDO and $H_2{}^{18}O$ atmospheric cycles using the NASA GISS general circulation model: The seasonal cycle for present-day conditions, *J. Geophys. Res.*, *92*(D12), 14,739–14,760, doi:10.1029/JD092iD12p14739.

Kalnay, E., et al. (1996), The NCEP/NCAR 40-year Reanalysis project, *Bull. Am. Meteorol. Soc.*, *77*, 437–471, doi:10.1175/1520-0477(1996)077<0437:TNYRP>2.0.CO;2.

Kanamitsu, M., et al. (2002a), NCEP dynamical seasonal forecast system 2000, *Bull. Am. Meteorol. Soc.*, *83*, 1019–1037, doi:10.1175/1520-0477(2002)083<1019:NDSFS>2.3.CO;2.

Kanamitsu, M., W. Ebisuzaki, J. Woolen, J. Potter, and M. Fiorino (2002b), NCEP/DOE AMIP-II Reanalysis (R-2), *Bull. Am. Meteorol. Soc.*, *83*, 1631–1643, doi:10.1175/BAMS-83-11-1631(2002)083<1631:NAR>2.3.CO;2.

Kang, I.-S., et al. (2002), Intercomparison of atmospheric GCM simulated anomalies associated with the 1997/98 El Niño, *J. Clim.*, *15*, 2791–2805, doi:10.1175/1520-0442(2002)015<2791:IOAGSA>2.0.CO;2.

Lee, J.-E., I. Fung, D. J. DePaolo, and C. C. Henning (2007), Analysis of the global distribution of water isotopes using the NCAR atmospheric

general circulation model, *J. Geophys. Res.*, *112*, D16306, doi:10.1029/2006JD007657.

Majoube, M. (1971a), Oxygen-18 and deuterium fractionation between water and steam (in French), *J. Chim. Phys.*, *68*, 1423–1436.

Majoube, M. (1971b), Fractionation in O-18 between ice and water vapor (in French), *J. Chim. Phys.*, *68*, 625–636.

Mathieu, R., D. Pollard, J. E. Cole, J. W. C. White, R. S. Webb, and S. L. Thompson (2002), Simulation of stable water isotope variations by the GENESIS GCM for modern conditions, *J. Geophys. Res.*, *107*(D4), 4037, doi:10.1029/2001JD900255.

Merlivat, L. (1978), Molecular diffusivities of $H_2{}^{16}O$, $HD^{16}O$ and $H_2{}^{18}O$ in gases, *J. Chim. Phys.*, *69*, 2864–2871, doi:10.1063/1.436884.

Merlivat, L., and J. Jouzel (1979), Global climatic interpretation of the deuterium oxygen 18 relationship for precipitation, *J. Geophys. Res.*, *84*, 5029–5033, doi:10.1029/JC084iC08p05029.

Moorthi, S., and M. J. Suarez (1992), Relaxed Arakawa-Schubert: A parameterization of moist convection for general circulation models, *Mon. Weather Rev.*, *120*, 978–1002, doi:10.1175/1520-0493(1992)120<0978:RASAPO>2.0.CO;2.

Noone, D. (2003), Water isotopes in CCSM for studying water cycles in the climate system, paper presented at CCSM Sci. Steering Comm., 8th Annual CCSM Workshop, Breckenridge, Colo., June.

Noone, D. (2006), Evaluation of hydrological cycles and processes with water isotopes: Report to GEWEX-GHP from the Stable Water-isotope Intercomparison Group (SWING), paper presented at First Pan-GEWEX Meeting, Eur. Space Res. and Technol. Cent., Frascati, Italy.

Noone, D., and I. Simmonds (2002), Associations between $\delta^{18}O$ of water and climate parameters in a simulation of atmospheric circulation 1979–1995, *J. Clim.*, *15*, 3150–3169, doi:10.1175/1520-0442(2002)015<3150:ABOOWA>2.0.CO;2.

Rimbu, N., T. Felis, G. Lohmann, and J. Paatzold (2006), Winter and summer climate patterns in the European-Middle East during recent centuries as documented in a northern Red Sea coral record, *Holocene*, *16*, 321–330, doi:10.1191/0959683606hl930rp.

Schmidt, G. A., G. Hoffmann, D. T. Shindell, and Y. Hu (2005), Modeling atmospheric stable water isotopes and the potential for constraining cloud processes and stratosphere-troposphere water exchange, *J. Geophys. Res.*, *110*, D21314, doi:10.1029/2005JD005790.

Schmidt, G. A., A. N. LeGrande, and G. Hoffmann (2007), Water isotope expressions of intrinsic and forced variability in a coupled ocean-atmosphere model, *J. Geophys. Res.*, *112*, D10103, doi:10.1029/2006JD007781.

Schneider, D. P., and D. C. Noone (2007), Spatial covariance of water isotope records in a global network of ice cores spanning twentieth-century climate change, *J. Geophys. Res.*, *112*, D18105, doi:10.1029/2007JD008652.

Stewart, M. K. (1975), Stable isotope fractionation due to evaporation and isotopic exchange of falling water drops, *J. Geophys. Res.*, *80*, 1138–1146.

Sturm, K., G. Hoffmann, B. Langmann, and W. Stichler (2005), Simulation of $\delta^{18}O$ in precipitation by the regional circulation model REMOiso, *Hydrol. Process.*, *19*, 3425–3444, doi:10.1002/hyp.5979.

Thompson, W. J., and J. M. Wallace (2000), Annular modes in the extratropical circulation. Part I: Month-to-month variability, *J. Clim.*, *13*, 1000–1016, doi:10.1175/1520-0442(2000)013<1000:AMITEC>2.0.CO;2.

Uemura, R., Y. Matsui, K. Yoshimura, H. Motoyama, and N. Yoshida (2008), Evidence of deuterium excess in water vapor as an indicator of ocean surface conditions, *J. Geophys. Res.*, doi:10.1029/2008JD010209, in press.

Webster, C. R., and A. J. Heymsfield (2003), Water isotope ratios D/H, $^{18}O/^{16}O$, $^{17}O/^{16}O$ in and out of clouds map dehydration pathways, *Science*, *302*, 1742–1745, doi:10.1126/science.1089496.

Welker, J. M., S. Rayback, and G. H. R. Henry (2005), Arctic and North Atlantic Oscillation phase changes are recorded in the isotopes ($\delta^{18}O$ and $\delta^{13}C$) of Cassiope tetragona plants, *Global Change Biol.*, *11*, 997–1002, doi:10.1111/j.1365-2486.2005.00961.x.

Wentz, F. J., L. Ricciardulli, K. Hilburn, and C. Mears (2007), How much more rain will global warming bring?, *Science*, *317*, 233–235, doi:10.1126/science.1140746.

Wolter, K., and M. S. Timlin (1998), Measuring the strength of ENSO events-How does 1997/98 rank?, *Weather*, *53*, 315–324.

Worden, J., D. Noone, and K. Bowman (2007), Importance of rain evaporation and continental convection in the tropical water cycle, *Nature*, *445*, 528–532, doi:10.1038/nature05508.

Yoshimura, K., and M. Kanamitsu (2008), Global dynamical downscaling of global reanalysis, *Mon. Weather Rev.*, *136*(8), 2983–2998.

Yoshimura, K., T. Oki, N. Ohte, and S. Kanae (2003), A quantitative analysis of short-term ^{18}O variability with a Rayleigh-type isotope circulation model, *J. Geophys. Res.*, *108*(D20), 4647, doi:10.1029/2003JD003477.

Yoshimura, K., T. Oki, and K. Ichiyanagi (2004), Evaluation of two-dimensional atmospheric water circulation fields in reanalyses by using precipitation isotopes databases, *J. Geophys. Res.*, *109*, D20109, doi:10.1029/2004JD004764.

Yoshimura, K., S. Miyazaki, S. Kanae, and T. Oki (2006), Iso-MATSIRO, a land surface model that incorporates stable water isotopes, *Global Planet. Change*, *51*, 90–107, doi:10.1016/j.gloplacha.2005.12.007.

M. Kanamitsu and K. Yoshimura, CASPO, Scripps Institution of Oceanography, University of California, MC0224, 9500 Gilman Drive, La Jolla, CA 92093-0224, USA. (k1yoshimura@ucsd.edu)

D. Noone, Department of Atmospheric and Oceanic Sciences, University of Colorado at Boulder, Campus Box 216, Boulder, CO 80303, USA.

T. Oki, Institute of Industrial Science, University of Tokyo, Building B, Room Be607, 4-6-1 Komaba, Meguro-ku, Tokyo 153-8505, Japan.